JOURNAL OF MATERIALS SCIENCE 31 (1996) 6395–6402

# Free-energies of the Ti–Ni, Fe–Ni and Mo–Ni alloys in relation to their behaviour under particle irradiation

R. H. DE TENDLER, C. RODRÍGUEZ*
*Instituto de Enseñanza Superior de Ezeiza and *Materiales y Combustibles Nucleares, Gerencia Centro Atómico Ezeiza, Comisión Nacional de Energía Atómica, Avda. del Libertador 8250, 1429 Buenos Aires, Argentina*

L. J. GALLEGO
*Departamento de Física de la Materia Condensada, Facultad de Física, Universidad de Santiago de Compostela, Santiago de Compostela, Spain*

J.A. ALONSO
*Departamento de Física Teórica, Facultad de Ciencias, Universidad de Valladolid, Valladolid 47011, Spain*

The metastable free-energy diagrams of the Ti–Ni, Fe–Ni and Mo–Ni systems were calculated at room temperature using a semiempirical theory based on thermodynamic considerations. Ti–Ni and Mo–Ni form equilibrium-ordered compounds that are destabilized by particle irradiation. Effectively, $Ti_2Ni$, TiNi, MoNi and $MoNi_3$ amorphize after irradiation. In the present work, this experimental behaviour is understood by considering the modification of the free-energy diagrams after particle irradiation. Conversely, in the Fe–Ni system, a metastable fcc solid solution evolves under irradiation towards ordered FeNi. In this system, according to our calculation, the free-energy of the amorphous phase is much higher than the free-energy of any other competing phase, so the amorphous phase cannot be produced. Each selected alloy has an intermetallic compound ($TiNi_3$, $FeNi_3$ and $MoNi_4$) which does not amorphize by particle irradiation and whose composition is close to the nickel-rich end of the phase diagram. According to the calculated free-energy diagrams, the reason for this impossibility of amorphization would be the competition of the terminal solid solution with the amorphous phase.

## 1. Introduction

In metallic alloys, some crystalline intermediate phases transform into the amorphous state after particle irradiation with electrons, ions or neutrons. Those intermediate phases, which have, in some cases, high melting temperatures, are linear intermetallic compounds with complex crystalline structures or compounds with an extended range of homogeneity and a simpler structure.

Experimental work on a variety of intermetallic compounds subjected to ion irradiation [1] has shown that the same binary alloy sometimes forms intermetallic compounds that remain crystalline after irradiation, and others that amorphize. These experimental results and our previous study on irradiated Zircaloy [2] led us to search for the reasons for the transformation of ordered crystalline phase → amorphous phase in the relative thermodynamic stability, as modified by irradiation, of the competing amorphous and crystalline phases (primary solid solutions and intermetallic compounds). Such relative stability is reflected in the diagrams of the free energy of the competing phases as a function of composition. The variety of alloys whose intermetallic compounds have been subjected to irradiation with different particles at several doses and temperatures [3] and the wealth of experimental information that has to be considered to analyse each system (i.e. features of the phase equilibrium diagram, ranges of amorphization by conventional methods and behaviour under irradiation) has compelled us to select three representative nickel alloys, Ti–Ni, Fe–Ni and Mo–Ni, to develop the present analysis. Each selected alloy has an intermetallic compound which does not amorphize by irradiation and whose composition is close to the nickel-rich end of the phase diagram, where there is a substantial solid solubility. Two of the alloys considered (Ti–Ni and Mo–Ni) form equilibrium-ordered compounds that are destabilized by irradiation and, on the contrary, in the Fe–Ni system, the metastable solid solution evolves under irradiation towards more stable ordered phases.

The free-energy diagrams, that we have calculated using Miedema's semi-empirical model, and the

0022–2461 

consideration of their modification after particle irradiation, makes possible the comprehension of the observed experimental behaviour of the Ti–Ni, Fe–Ni and Mo–Ni alloys under irradiation.

## 2. Calculation of the metastable free-energy diagrams

We have calculated the free-energy diagrams of the Ti–Ni, Fe–Ni and Mo–Ni alloys at 298 K. Those diagrams contain the free-energy curves of some stable and metastable phases (intermetallic compounds, metastable solid solutions and amorphous alloys), which have been calculated by using a semi-empirical theory due to Miedema and co-workers [4–12] and further developed by López *et al.* [13]. Detailed descriptions of the theory are given in the literature [2, 4–13]. In the present section we only give a brief outline of this procedure.

The free-energy of formation of a crystalline substitutional solid solution with respect to the pure metals is given by the following equation

$$\Delta G_s = \Delta H_s - T\Delta S_{ideal} - T\Delta S_{str} \quad (1)$$

where $\Delta H_s$ is the enthalpy of formation, $\Delta S_{ideal}$ is the ideal entropy of formation, and $\Delta S_{str}$ is a structural contribution to the entropy of formation. These terms are now discussed separately. The enthalpy of formation contains chemical, elastic and structural contributions

$$\Delta H_s = \Delta H_c + \Delta H_e + \Delta H_{str} \quad (2)$$

The chemical contribution, $\Delta H_c$, is due to the electron redistribution that occurs when atoms of two different types mix together. This enthalpy is controlled by (a) the difference between the electronegativities of the two components, and (b) the difference of electron density at the boundary of the atomic cells [4, 10]. The expression for $\Delta H_c$ contains a parameter, $\gamma$, which specifies the degree of chemical order in the alloy. For disordered substitutional solid solutions, the value of this parameter is $\gamma = 0$.

The elastic contribution, $\Delta H_e$, arises from the size mismatch between solute and host atoms. This contribution has been calculated using classical elasticity theory [10]. The shear and bulk moduli of the component metals are ingredients required to calculate $\Delta H_e$. In our case, the shear and bulk moduli of fcc Ni, hcp Ti and bcc Mo have been taken from Gschneidner [14].

The structural contribution, $\Delta H_{str}$, reflects the fact that there is a systematic variation of the crystal structure as the number of valence electrons changes across each transition metal period. Similar structural changes are then expected when the effective number of valence electrons is changed by the addition of the solute atoms. Relative stability functions have been computed by Niessen and Miedema for the three main crystallographic structures (hcp, fcc and bcc) for non-magnetic [6] and ferromagnetic metals [11], and $\Delta H_{str}$ is computed from those stability functions. The reference stability at each concentration has been defined by the linear interpolation between the lattice stabilities of the two pure metals in their stable structures at 298 K (exceptions to this criterion will be indicated in the discussion of the corresponding alloys).

$\Delta S_{str}$ was defined by Rodríguez *et al.* [2] as a weighted average of the entropy changes associated with the structural transformation of each of the pure metals from its reference structure into the structure of the solid solution, (hcp, fcc or bcc). Those entropy values for the pure metals have been taken from tables presented by Kaufman and Bernstein [15].

The free-energy of formation of the amorphous alloy with respect to the pure crystalline metals is [13]

$$\Delta G_a = \Delta H_c - T\Delta S_{ideal} + x_i(\Delta G_{as})_i + x_{Ni}(\Delta G_{as})_{Ni} \quad (3)$$

where i represents titanium, iron or molybdenum.

The two terms containing $\Delta G_{as}$ give the difference in free-energy between the undercooled liquid and crystalline phases of each of the two pure metals, and the part $\Delta H_c - T\Delta S_{ideal}$ is the free-energy of mixing with respect to the "liquid" metals. For the parameter $\gamma$, appearing in $\Delta H_c$ and specifying the degree of chemical short-range order in the amorphous alloy, we have taken the value $\gamma = 5$, as was previously established by Weeber [12]. This value is halfway between the values $\gamma = 0$ (valid for random alloys) and $\gamma = 8$ (describing fully ordered compounds). Elastic and structural terms are, evidently, not necessary in the case of amorphous alloys. Finally, the free-energies of formation of the intermetallic compounds are just the enthalpies of formation (the chemical term with $\gamma = 8$) reported elsewhere [10].

## 3. Discussion

### 3.1. Ti–Ni

The calculated free-energy diagram of this alloy is shown in Fig. 1. The phases compared are the amorphous alloy, the solid solutions, and the three ordered compounds $Ti_2Ni$, TiNi and $TiNi_3$. Three different regions can be observed in the curve for solid solutions. In region 1, corresponding to a nickel concentration $x(Ni) \leqslant 5$ at %, the structure is hcp, which is the structure of pure titanium at 298 K. When the nickel concentration increases above this limiting value, the structural term turns a bcc solid solution more stable than the terminal hcp phase. The bcc is then the structure of the solid solution in region 2. Finally, for $x(Ni) \geqslant 45$ at %, that is in the nickel-rich side, the structure of the solid solution is the fcc structure of pure nickel, again due to $\Delta H_{str}$.

In constructing the curve for solid solutions we have calculated the structural contribution, $\Delta H_{str}$, using the lattice stability values for non-magnetic metals [6] because at 298 K only alloys with a nickel content higher than 92.7 at % are ferromagnetic [16]. At this temperature, the reference structural stability was defined by pure hcp Ti and fcc Ni. The structural contribution for the terminal solid solutions based on hcp Ti or fcc Ni was then calculated by using the lattice stability functions as in the standard Miedema method [2, 16]. However, when the same method is used to calculate $\Delta H_{str}$ for the bcc structure, the

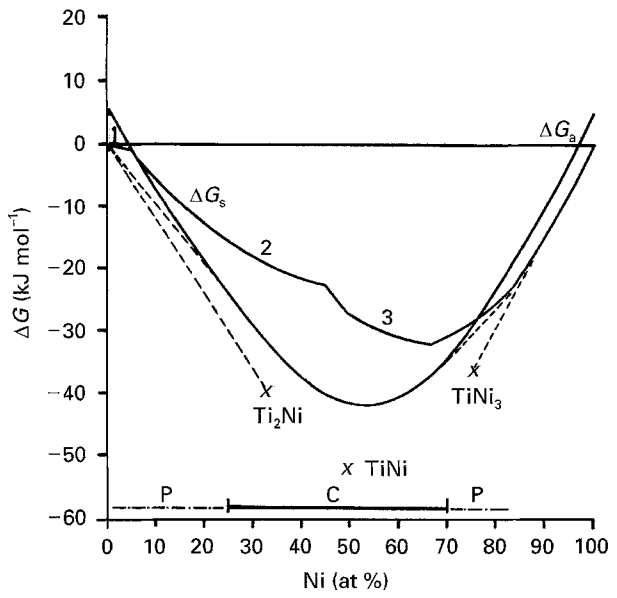


*Figure 1* Metastable free-energy diagram of the Ti–Ni system at 298 K, showing the free-energies of formation of the different phases as functions of the nickel atomic concentration. Those phases are; s, solid solution; a, amorphous alloy; x, intermetallic compounds. In the solid solution curve, the concentrations 5 at % Ni, and 45 at % Ni separate the hcp (1), bcc (2) and fcc (3) phases. The regions labelled C and P indicate, respectively, the predicted complete and partial glass-forming composition ranges. Common tangents to the free-energy curves of several phases have been drawn (– – –).

stability of this phase is overestimated. In effect, Miedema's method predicts that the eutectoid reaction $\beta Ti \leftrightarrows \alpha Ti + Ti_2Ni$ occurs at room temperature, whereas it has been effectively observed at 1038 K [16]. βTi and αTi in the above equation indicate the terminal solid solutions based on the bcc (high-temperature) and hcp (low temperature) structures of titanium. As an alternative that allows a correct description of the phase equilibria, we have estimated $\Delta H_{str}$ for the bcc solid solution as a linear interpolation between the lattice stabilities of pure bcc titanium and bcc nickel. This approach was earlier suggested by Miedema and Niessen [8].

The free-energy diagram of Fig. 1 predicts, at the titanium-rich corner, the existence of the phase mixture Ti (hcp) + $Ti_2Ni$ and a negligible solid solubility of nickel in Ti (hcp). Both predictions are in good agreement with the assessed phase diagram given elsewhere [16]. In the range of compositions contained between $Ti_2Ni$ and $TiNi_3$, the predicted most stable phases are the compound TiNi(B2) and the two-phase mixtures $Ti_2Ni$–TiNi and TiNi–$TiNi_3$. Then TiNi(B2) is predicted to be a stable phase at low temperature. In the assessed phase diagram [16], a single-phase region with ordered bcc structure (CsCl type), enclosing the equiatomic composition is shown at high temperatures. According to Murray [16], there is agreement in the literature on the extent of the single-phase region at temperatures higher than 1173 K. The phase boundary on the titanium-rich side is essentially vertical, but on the nickel-rich side the homogeneity range decreases sharply with temperature. The presence of the eutectoid reaction $TiNi \rightleftharpoons Ti_2Ni + TiNi_3$ at 903 ± 15 K in the assessed phase diagram is opposed to the extension of the TiNi phase field down to lower temperatures, as predicted by Miedema's model. The existence of this eutectoid reaction has been a source of controversy [16]. In recent work, looking at the microstructures that result from sample preparation [1, 17, 18], the presence of TiNi(B2) coexisting in partial equilibrium with $Ti_2Ni$ and $TiNi_3$ was observed at low temperature. The starting material used by Brimhall and Kissinger [18] for irradiation experiments was a commercial Ti–Ni alloy of nominal composition 49.5 at % Ti that was furnace cooled after annealing at 1273 K. This alloy consisted of isolated particles of $Ti_2Ni$ in a TiNi matrix. Our prediction from Fig. 1 is in good agreement with these recent experimental observations.

In the experimental phase diagram [16] the high solid solubility of titanium in the fcc Ni (14 at % at 1573 K) diminishes with decreasing temperature down to an extrapolated value of 5 at % at room temperature. The Ni (fcc) field is followed by a two-phase field Ni(fcc) + $TiNi_3$. The free-energy diagram of Fig. 1 predicts, at room temperature, a maximum solid solubility of 7 at % Ti in fcc Ni resulting from the equilibrium between the fcc solid solution and the compound $TiNi_3$. This solubility compares well with the value 5 at % Ti mentioned above. Fig. 1 also establishes the existence of the two-phase field Ni(fcc) + $TiNi_3$.

Crystalline powders of nickel and titanium have been mechanically alloyed by high-energy ball milling in an inert atmosphere at $T < 240$ K. The resulting powder was amorphous between 28 and 72 at % Ni, and outside this range it consists of a two-phase mixture of the amorphous phase and the crystalline terminal solid solutions [19]. From an analysis of the lattice parameters, the extended "metastable" solid solubility of titanium in fcc Ni was estimated to be approximately 28 at % Ti, which is significantly larger than the equilibrium value of 5 at % Ti. In Ti–Ni alloys splat cooled at rates $10^7$–$10^8$ K $s^{-1}$, Polesya and Sluipchenko [20] observed an extended solubility of titanium in nickel of 22.3 at % Ti. If we admit that the formation of the ordered compounds can be kinetically by-passed, then in the diagram of Fig. 1 the common tangents to the free-energy curves of the amorphous alloy and the terminal solid solutions define a complete amorphization range that extends between 25 at % Ni and 70 at % Ni. At the nickel-rich end, the common tangent defines an extended metastable solid solubility of 18 at % Ti in fcc Ni. The partial amorphization range extends, on the titanium-rich end, between pure titanium and the amorphous alloy with 25 at % Ni. At the nickel-rich end, the partial amorphization range corresponds to the two-phase mixture of a metastable extended solid solution (18 at % Ti in nickel) and the amorphous phase with 70 at % Ni. In conclusion, the theoretical range of complete amorphization of Fig. 1 agrees well with the ball-milling results reported elsewhere [19]. Also in agreement with the experimental observations, the model predicts an extended "metastable" range of solubility of titanium in fcc Ni much larger than the equilibrium solubility. It should be noticed that

a reasonable evaluation of the limiting solubility in rapid solidification processes is provided by the composition where the free-energy curves of the solid solution and the amorphous phase intersect each other [21]. The limit obtained from Fig. 1 applying this criterion is 24 at % Ti, which agrees well with the limiting solubility (22.3 at % Ti) measured by splat-cooling [20].

By-passing the formation of ordered compounds during the fast quenching experiments is sometimes difficult. For example, Buschow prepared Ti–Ni amorphous alloys containing 24, 30, 35, 40, 58, 60, 62 and 64 at % Ni by arc-melting followed by melt-spinning [22], and he observed the tendency to form glasses to weaken in the range between 40 and 58 at % Ni. Similarly, Pedraza *et al.* [23] pointed out that TiNi alloys of near equiatomic composition remain crystalline after being melted by irradiation with nanosecond laser pulses. In both cases, the difficulty for amorphization occurs at compositions near to that of the equiatomic compound, which is stable up to a high temperature and, furthermore, has a wide range of composition.

The crystallization products of the amorphous alloys with 24 and 30 at % Ni are given by the two-phase mixture h c p Ti + $Ti_2Ni$ [22]. The experiments also reveal that amorphous alloys with 35 at % Ni and 40 at % Ni crystallize, respectively, into the $Ti_2Ni$ compound and the two-phase mixture $Ti_2Ni$ + TiNi [22]. The free-energy diagram of Fig. 1 predicts a crystallization behaviour in agreement with these observations.

Crystalline alloys that become amorphous by some conventional techniques possess intermediate phases that are also susceptible to be amorphized by irradiation with energetic particles like electrons, protons, ions and neutrons. Stoichiometric compounds, phases with high melting temperatures, and solid solutions with a narrow composition range and a high degree of long-range order, are often amorphized when irradiated, although exceptions to this rule are frequently reported. Instead, pure metals and disordered solid solutions with wide composition range are more difficult or impossible to amorphize. In thermodynamic-based discussions of the crystalline to amorphous transformation it is generally assumed that the increase of free-energy of the crystal associated with the build up of point defects, defect complexes [24] and chemical disorder created by high-energy particle irradiation, is stored in the lattice and provides the driving force for the transformation. The transformation should occur, by some yet unspecified mechanism, when the free energy of the perturbed crystalline phase becomes higher than the free energy of the amorphous phase.

According to the compilation by Okamoto and Meshii [3] partially reproduced in Table I, we see that $Ti_2Ni$ and TiNi become amorphous by electron irradiation even above room temperature, whereas $TiNi_3$ remains crystalline. Samples where $Ti_2Ni$ was present as discrete particles in a TiNi(B2) matrix were bombarded with 2.5 MeV $Ni^+$ ions at ambient temperature and above [1, 17,18]. All specimens received

TABLE I Amorphization of Ti–Ni compounds under electron irradiation [3]

| Alloy | Structure[a] | $e^-$ energy (MeV) | $T_{irrad}$[b] (K) | C/A[c] |
|---|---|---|---|---|
| $TiNi_3$ | $D0_{24}$ | 1.2 | 90–300 | C |
| TiNi | $B2$ | 0.5–2 | 193–473 | A |
| | | 2 | 50–393 | A |
| | | 1.5 | 293 | A |
| | | 0.6–1.5 | 90–300 | A |
| $Ti_2Ni$ | $E9_3$ | 2 | 160 | A |

[a] Structure of the starting compound.
[b] $T_{irrad}$: temperature of irradiation.
[c] C, crystalline; A, amorphous.

doses $\leqslant 1$ d.p.a. (displacement per atom) and of 10 d.p.a. Both phases transformed easily into the amorphous state after doses $< 1$ d.p.a., although $Ti_2Ni$ was reported somewhat harder to amorphize. Samples of both TiNi and $TiNi_3$ present as extended phases [1] were irradiated to doses up to 10 d.p.a. At doses of 1 d.p.a. the sample consisted of a mixture of crystalline $TiNi_3$ grains and amorphous TiNi grains. $TiNi_3$ remained crystalline up to doses of 10 d.p.a. [1]. From Fig. 1, we see that if the free-energy of $Ti_2Ni$ and TiNi can be increased to above a critical value, both phases can be transformed into the amorphous phase. Also from Fig. 1, we see that at the composition of $TiNi_3$ the formation of an amorphous phase competes with the formation of the Ni (f c c) solid solution. Attaining equilibrium between those two phases may be difficult because this would imply separation into two phases of different composition and this requires massive diffusion. So the resistance of the $TiNi_3$ compound to amorphization seems to be related to this difficulty.

## 3.2. Fe–Ni

Fig. 2 shows the calculated free-energy diagram of the Fe–Ni alloy at 300 K. The phases compared are the three intermetallic compounds $Fe_3Ni$, FeNi and $FeNi_3$, the amorphous phase and the solid solutions. Because pure b c c Fe and f c c Ni are ferromagnetic, as well as the b c c and f c c solid solutions formed by these two metals [25], the structural contribution, $\Delta H_{str}$ (see Equation 2) has been calculated by using the lattice stability functions for metals in the ferromagnetic state [11]. The reference structural stability in Fig. 2 was defined by pure b c c Fe and pure f c c Ni. The curve for the solid solutions can be separated in two regions. Between 0 and 30 at % Ni (region 1 in the figure) the solid solution ($\alpha$ phase) has the b c c structure of iron, but beyond that limit the structural term stabilizes the $\gamma$ phase with the f c c structure of nickel (region 2 in the figure).

The calculation indicates that the $Fe_3Ni$ and FeNi compounds are more stable, although only marginally, than a mixture of $FeNi_3$ and the iron-based b c c solid solution. This result may serve to interpret the conflicting experimental reports about the existence of the compounds $Fe_3Ni$ and FeNi. It is not clear from

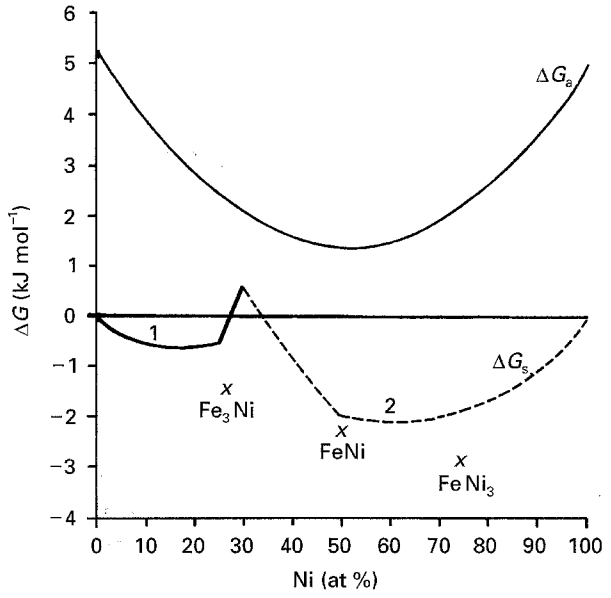


*Figure 2* Metastable free-energy diagram of the Fe–Ni system at 300 K, showing the free-energies of formation of the different phases as functions of the nickel atomic concentration. Those phases are: s, solid solution; a, amorphous alloy; x, intermetallic compounds. In the solid solution curve, the concentration 30 at % Ni separates the bcc (1) and fcc (2) phases.

those reports if these two are stable or metastable compounds. The equilibrium phase diagram published elsewhere [25] proposes the two-phase mixture ($\alpha$ + $FeNi_3$) as forming the low-temperature equilibrium state for concentrations between 0 and 70 at % Ni. However, because diffusion-controlled transformations are very slow at low temperatures, it may occur that the equilibrium phases could not be obtained within laboratory times, and that the evolution towards the equilibrium phases could only be completed when atomic diffusion is enhanced by irradiation with high-energy particles [26, 27], or for very long times, such as those occurring during the cooling of Fe–Ni meteorites [28]. The metallic phases of meteorites are predominantly composed of iron with 4.8–48.8 at % Ni. These have undergone extremely slow cooling below 773 K at rates in the range $10^{-1}$–$10^{3}$ K per million years, and as a result, a phase separation into fcc regions with a higher nickel content (~46.7–48.8 at % Ni) and bcc regions with a poorer nickel content (~4.8 at % Ni) has been observed [28]. The last ones may, in turn, transform into martensite, whereas the nickel-rich regions are often ordered with the FeNi $L1_0$ superlattice structure.

Samples of the $\gamma$ phase (the fcc solid solution) with equiatomic concentration were irradiated by neutrons or electrons in the presence of a magnetic field [26, 27], and transformed into a mixture of a disordered $\gamma$ phase and ordered FeNi. A single crystal with equiatomic concentration, heated to 568 K while being subjected to a uniform magnetic field of 2500 Oe, was also irradiated with neutrons of more than 1 MeV energy, at a dose of $2.1 \times 10^{19}$ neutrons $cm^{-2}$ [26], and by electrons of 2 MeV [27]. The X-ray analysis of the bombarded sample confirmed the presence of an ordered structure of the AuCu-type. The critical temperature of the ordered phase is 593 K, and the ordering induces a large magnetic anisotropy. The existence of $Fe_3Ni$ precipitates finely dispersed in an fcc matrix has been reported in the study of an Invar alloy [29] although this result has not been confirmed later. Recent microstructural observations and measurements made on Fe–Ni meteorites [30] have been found compatible with a phase diagram obtained from thermodynamic calculations including magnetic contributions to the free-energy [31]. The new phase diagram proposed [30] shows a low-temperature equiatomic FeNi phase ordered up to 573 K. Furthermore, the formation of $Fe_3Ni$ has been suggested, although its identification is not certain. Our prediction from Miedema's model is that the free energies of FeNi and $Fe_3Ni$ are very close to those for a mixture of $FeNi_3$ and a dilute iron-based bcc solid solution, so a strong competition between the compounds and the two-phase mixture can be expected. Further experimental work and more accurate theoretical modelling are required to settle this question.

At high temperatures, above 1185 K, the equilibrium phase in the Fe–Ni system is an fcc solid solution ($\gamma$ phase) which extends continuously over the whole composition range. However, below that temperature the bcc solid solution ($\alpha$ phase) based on the low-temperature bcc structure of the iron competes with the $\gamma$ phase, and a two-phase $\alpha + \gamma$ region develops. This two-phase mixture is well explained by our model. For instance, at the room temperature used to construct Fig. 2 the two-phase region can be found by drawing the common tangent to the two branches, labelled 1 and 2, of the $\Delta G_s$ curve. This produces a two-phase region for compositions between 5 at % Ni and 50 at % Ni. These limits are not very different from the result that one obtains by extrapolating the experimental two-phase region of the standard equilibrium phase diagram of Swartzendruber *et al.* [25] to this temperature. The reason for comparing with the extrapolated experimental result is because at room temperature the existence of the compounds has to be considered. As we can observe in Fig. 2, the $\gamma$ phase is totally suppressed at low temperature by the presence of the compounds. There are a number of experimental reports [32–34] which indicate that the Fe–Ni phase diagram may be more complex than the one usually accepted [25]. Those reports suggest that the fcc solid solution is intrinsically unstable at low temperature. We first refer briefly to those experiments and then show that the calculated free-energies support this possibility.

Irradiation of an Invar alloy containing 34 at % Ni with 2 MeV protons up to a dose of 0.5 d.p.a. and at temperatures higher than 873 K, resulted in compositional fluctuations between 28.5 and 36.5 at % Ni, that is formation of crystallites of these two compositions with an effective crystallite radius of 220 nm [32]. This can be ascribed to the thermodynamic instability of the $\gamma$ phase, accelerated by radiation-enhanced diffusion [32]. Phase separation in Invar alloys irradiated by high doses of $Ne^+$ and $Ar^+$ ions at room temperature and at 473 K has also been reported [33].

Compositional fluctuations between 25 and 50 at % Ni have been recently observed by irradiating alloys of 35 at % Ni with ions ($10^{-2}$ d.p.a. $s^{-1}$) and neutrons ($10^{-8}$ d.p.a. $s^{-1}$) at temperatures up to 800 K [34]. In the same work [34], compositional fluctuations between 30 and 40 at % Ni have been induced by annealing at 898 K for a period of 230 days. This behaviour has been attributed to a natural evolution due to the thermodynamic instability of the γ phase, accelerated by the irradiation.

Fig. 3 shows the calculated free-energy of formation for the austenitic γ Fe–Ni solid solution at three temperatures: 300, 898 and 998 K. The reference structural stability for these curves was defined by pure fcc Fe and pure fcc Ni. According to the present calculation, the γ phase presents a miscibility gap which at 300 K extends between 0 and 50 at % Ni. This low temperature is not very interesting for the reasons discussed above. The free-energy curves at 898 and 998 K also indicate that in the range of compositions roughly between 10 at % Ni and 50 at % Ni, the fcc alloy would separate into fcc crystallites with ~10 at % Ni and ~50 at % Ni. This result is consistent with the miscibility gap in the γ field and the compositional fluctuations observed by some workers [32, 34], as well as with the spinodal decomposition observed at low temperature [33].

Fig. 2 also shows that the free-energy of the amorphous alloy, $\Delta G_a$, is much higher than the free-energies of the other phases, or phase mixtures. In fact the amorphous phase is intrinsically unstable. This indicates that amorphization should be very difficult. In effect, experiments have shown that amorphization of this alloy requires extreme conditions such as vapour-quenching at very low temperatures (4.2 K) [35]. On the other hand, the failure to produce an amorphous phase by irradiating the $FeNi_3$ intermetallic compound with high-energy electrons [36] is also consistent with the free-energy diagram. The disordered fcc solid solution stands as an available phase requiring a much lower energy increase than the formation of the amorphous alloy of the same composition.

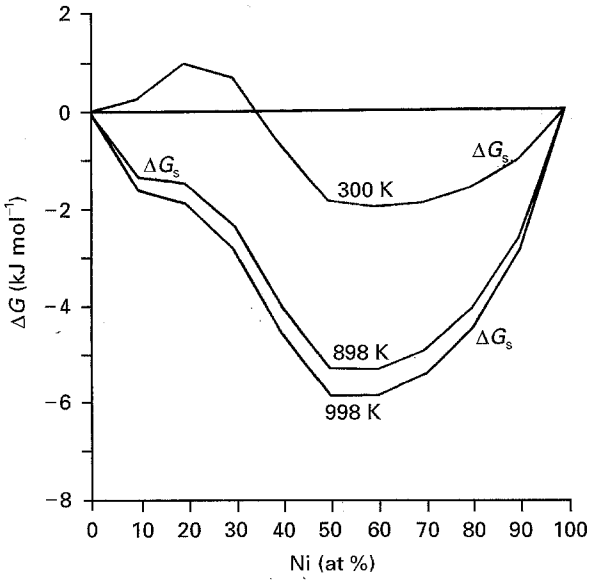


*Figure 3* Free-energy of the fcc Fe–Ni solid solution at 300, 898 and 998 K, with respect to the pure fcc components. s: solid solution.

## 3.3. Mo–Ni

Fig. 4 shows the free-energy diagram of Mo–Ni alloys at 298 K. This temperature is the Curie temperature, $T_c$, for a solid solution of molybdenum in nickel containing 94.4 at % Ni, and $T_c$ diminishes as the nickel content decreases [37]. Accordingly, the structural contribution, $\Delta H_{str}$ to $\Delta G_s$ has been calculated by using the lattice stability functions for non-magnetic metals [6]. The reference structural stability was defined by bcc Mo and fcc Ni. The free-energy curve of the solid solution, $\Delta G_s$, is composed of two branches. The first one is the molybdenum-based bcc solid solution between 0 and 19 at % Ni and, beyond this composition, the second branch is the fcc solid solution. According to the assessed phase diagram of Mo–Ni, this system shows a peritectic and a eutectic reaction, three incongruently melting intermetallic compounds (MoNi, $MoNi_3$ and $MoNi_4$), extensive solid solubility of molybdenum in fcc Ni (at least above 973 K) and a very limited terminal solid solubility of nickel in bcc Mo [37]. MoNi appears as the most stable intermetallic compound in the calculated free-energy diagram of Fig. 4, in agreement with the experimental result which shows that this is the intermetallic with the highest temperature of invariant reaction (decomposition reaction) [37]. The free-energy diagram also displays a negligible solid solubility of nickel in bcc Mo, in accordance with the negligible solid solubility that the experimental solvus line displays even at much higher temperatures [37]. Our calculation also predicts a negligible low-temperature

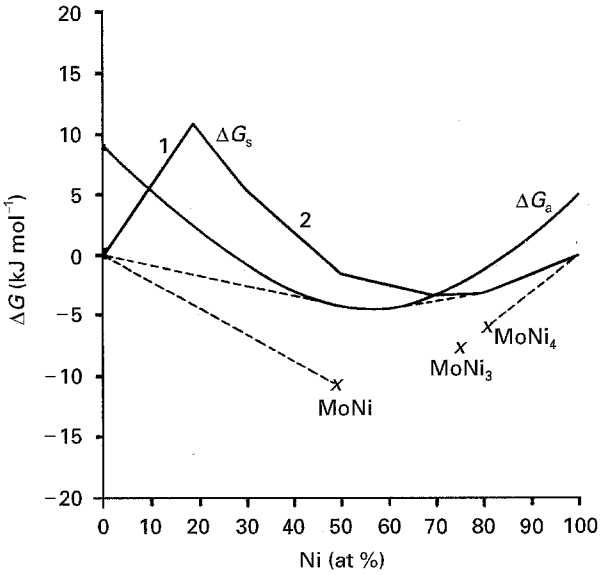


*Figure 4* Metastable free-energy diagram of the Mo–Ni system at 298 K, showing the free-energies of formation of the different phases as functions of the nickel atomic concentration. Those phases are: s, solid solution; a, amorphous alloy; x, intermetallic compounds. In the solid solution curve, the concentration 19 at % Ni separates the bcc (1) and fcc (2) phases. Common tangents to the free-energy curves of several phases have been drawn (---).

solid solubility of molybdenum in fcc Ni. The experimental information on this point is not clear-cut. Only at much higher temperatures has the extent of solid solubility of molybdenum in nickel been measured, and an extrapolation of the solvus line to low temperature is required. There are conflicting extrapolations [38]. The form of the solvus line recommended by Okamoto [38] leads to an extrapolation consistent with our prediction of very low solid solubility at low temperature. Evidently our calculation predicts that the solubility of molybdenum in nickel increases with increasing temperature, because the entropic contribution shifts the free-energy of the solid solution down relative to that for the $MoNi_4$ compound.

The prediction from our calculations is that bcc Mo is followed by the two-phase equilibrium bcc Mo + MoNi, and the fcc nickel-based solid solution is followed by the phase mixture of fcc solid solution + $MoNi_4$, in good agreement with the assessed phase diagram [37].

The common tangents to the free-energy curves of the metastable fcc solid solution and of the amorphous phase at the nickel-rich end, and to the curves of the amorphous phase and the terminal bcc Mo solid solution at the molybdenum-rich end define a narrow range of complete amorphization that extends between 48 and 62 at % Ni. Outside this range, Fig. 4 predicts the existence of regions of partial amorphization which are two-phase fields of metastable equilibrium between almost pure bcc Mo and an amorphous alloy containing 48 at % Ni at one end, and between an extended fcc solid solution containing 20 at % Mo and a 62 at % Ni amorphous alloy at the other end. Literature reporting experimental information on the glass formation in nickel alloys [39] states that rapid quenching from the melt of Mo–Ni alloys of unspecified composition at cooling rates varying from $10^5$–$10^6$ K $s^{-1}$ do not lead to the formation of metallic glasses. However, recent work by Wang *et al.* [40] reports that an amorphous phase was obtained by ball milling in Mo–Ni alloys containing 40, 50 and 62 at % Ni, whereas the alloys containing 70 and 80 at % Ni consisted of nickel solid solution. This result is consistent with the diagram in Fig. 4. Furthermore, amorphous Mo–Ni alloys have been obtained by ion mixing [41]. Multilayers with overall composition $Mo_{35}Ni_{65}$, $Mo_{50}Ni_{50}$ and $Mo_{65}Ni_{35}$ became amorphous under bombardment at room temperature by 300 keV $Xe^+$ at certain doses. The equiatomic composition required the lowest dose and was therefore optimum for glass formation [42]. These results are compatible with the free-energy diagram of Fig. 4 because, if the formation of the intermetallic compounds is kinetically avoided, then the amorphous phase is the one with the lowest free-energy at the three concentrations studied in this experiment. In particular, the equiatomic concentration, which required the lowest dose of the three compositions, lies within the range of complete amorphization predicted from Fig. 4. A full analysis of the irradiation and post-irradiation thermal annealing behaviour of those samples has been given elsewhere [43].

TABLE II Data on the amorphization of Mo–Ni compounds under electron irradiation [3]

| Alloy | Structure[a] | $e^-$ energy (MeV) | $T_{irrad}$[b] (K) | C/A[c] | Reference |
|---|---|---|---|---|---|
| $MoNi_4$ | $D1_a$ | 1 | 50–1050 | C | [45] |
| $MoNi_3$ | $A3$ | 2 | 293 | PA | [46] |
| MoNi | Tetragonal | 2 | 160 | A | [44] |

[a] Structure of the starting compound.
[b] $T_{irrad}$, temperature of irradiation.
[c] C, crystalline; PA, partially amorphous; A, totally amorphous.

The data in Table II have been taken from the review paper by Okamoto and Meshii [3] and it lists the results of experiments on electron irradiation of the intermetallic compounds in the Mo–Ni system. Mori *et al.* [44] have irradiated $Mo_{52}Ni_{48}$ specimens with 2 MeV electrons in an ultra-high voltage electron microscope. Changes in the microstructure as well as in the selected-area diffraction pattern were monitored *in situ* during irradiation. The irradiation temperature was fixed at around 160 K and the electron flux at $1 \times 10^{24}$ e $m^{-2}$ $s^{-1}$, throughout the experiment. MoNi (tetragonal) undergoes a crystalline → amorphous transition upon irradiation. Banerjee *et al.* [45], have reported and discussed an order–disorder transformation in $MoNi_4$ after electron irradiation, but $MoNi_4$ remains crystalline. Finally, according to Yamamoto *et al.* [46], $MoNi_3$ turns into a partially amorphous sample under electron irradiation. The behaviour displayed by the three intermetallic compounds under electron irradiation is well understood from Fig. 4. The free-energy diagram shows that at the equiatomic concentration the preferred metastable phase is the amorphous alloy, while at the concentration corresponding to $MoNi_4$ the preferred metastable phase is the fcc Ni-based solid solution and a mixture of amorphous alloy and solid solution is the preferred phase at the composition of $MoNi_3$.

## 4. Conclusion

In the calculated free-energy diagram of Ti–Ni alloy (Fig. 1) the theoretical solid solubility limits for both the titanium-rich and nickel-rich sides are in good accordance with the assessed phase diagram [16] and the complete and partial amorphization ranges predicted by the model agree well with the ranges of amorphization measured in experiments of mechanical mixing [19]. The free-energy diagram predicts that ion and electron irradiations can promote the amorphization of $Ti_2Ni$ and TiNi but not of $TiNi_3$ that will remain crystalline. This behaviour has been experimentally observed [17, 18]. We conclude that free-energy calculations using the Miedema's model predict the observed behaviour of $Ti_2Ni$, TiNi and $TiNi_3$ after irradiation.

A similar calculation shows that the three intermetallic compounds, $Fe_3Ni$, FeNi and $FeNi_3$ should be present in the Fe–Ni equilibrium phase diagram (Fig. 2). We argue that kinetic barriers may inhibit the formation of $Fe_3Ni$ and FeNi. The amorphous phase cannot be obtained in the Fe–Ni system because the

free energy of formation of this phase is much higher than that of any other possible phases.

Miedema's model predicts that MoNi and $MoNi_3$ will transform into the amorphous and partially amorphous phases, respectively, after electron irradiation. Instead, $MoNi_4$ will remain crystalline (Fig. 4). These predictions agree well with the experiments reported elsewhere [44–46].

The three alloy systems studied here present different behaviour: a great variation of amorphization ranges and the appearance, after irradiation, of different metastable phases. The different behaviour is well interpreted using Miedema's model. In particular, concerning the different propensity for amorphization of the intermetallic compounds under irradiation, it has been found that the competition of the terminal solid solution with the amorphous phase could be the reason for the impossibility of amorphization of the compounds $TiNi_3$, $FeNi_3$ and $MoNi_4$ reported in the literature [1, 36, 45].

## Acknowledgements

The authors thank A. J. Pedraza for fruitful discussions. This work has been supported by DGICYT (Grant PB 92-0645).

## References

1. J. L. BRIMHALL, H. E. KISSINGER and L. A. CHARLOT, *Rad. Eff. Def. Solids* **77** (1983) 237.
2. C. RODRIGUEZ, R. H. DE TENDLER, L. J. GALLEGO and J. A. ALONSO, *J. Mater. Sci.* **30** (1995) 196.
3. P. R. OKAMOTO and M. MESHII, "Science of Advanced Materials", Vol. **33**, edited by H. Wiedersich and M. Meshii (ASM International, Metals Park, OH, 1990).
4. A. K. NIESSEN, F. R. DE BOER, R. BOOM, P. F. DE CHÂTEL, W. C. M. MATTENS and A. R. MIEDEMA, *Calphad* **7** (1983) 51.
5. A. R. MIEDEMA and A. K. NIESSEN, *ibid.* **7** (1983) 27.
6. A. K. NIESSEN and A. R. MIEDEMA, *Ber. Bunsenges Phys. Chem.* **87** (1983) 717.
7. P. I. LOEFF, A. W. WEEBER and A. R. MIEDEMA, *J. Less-Common Metals* **140** (1988) 299.
8. A. R. MIEDEMA and A. K. NIESSEN, *Trans. Jpn Inst. Metals* **29** (1988) 209.
9. J. G. VAN DER KOLK, A. R. MIEDEMA and A. K. NIESSEN, *J. Less-Common Metals* **145** (1988) 1.
10. F. R. DE BOER, R. BOOM, W. C. M. MATTENS, A. R. MIEDEMA and A. K. NIESSEN, "Cohesion in Metals, Transition Metal Alloys" (North-Holland, Amsterdam, 1988).
11. A. K. NIESSEN, A. R. MIEDEMA, F. R DE BOER and R. BOOM, *Physica B* **151** (1988) 401.
12. A. W. WEEBER, *J. Phys. F Metal Phys.* **17** (1987) 809.
13. J. M. LÓPEZ, J. A. ALONSO and L. J. GALLEGO, *Phys. Rev.* **B36** (1987) 3716.
14. K. A. GSCHNEIDNER Jr, *Solid State Phys.* **16** (1964) 275.
15. L. KAUFMAN and H. BERNSTEIN, "Computer Calculation of Phase Diagrams" (Academic Press, New York, London, 1970).
16. J. L. MURRAY, in "Phase Diagrams of Binary Nickel Alloys", edited by P. Nash, (ASM International, Materials, Park, OH, 1991) p. 342.
17. P. J. MAZIASZ and D. F. PEDRAZA, J. P. SIMMONS, N. H. PACKAN, *J. Mater. Res.* **5** (1990) 932.
18. J. L. BRIMHALL and H. E. KISSINGER, *Rad. Effects Def. Solids* **90** (1985) 241.
19. R. B. SCHWARZ, R. R. PETRICH and C. K. SAW, *J. Non-Cryst. Solids* **76** (1985) 281.
20. A. F. POLESYA and L. S. SLUIPCHENKO, *Russ. Metall.* **6** (1973) 103.
21. T. B. MASSALSKI, in "Proceedings of the Fourth International Conference on Rapidly Quenched Metals", edited by M. Masumoto and S. Suzuki (Japan Institute of Metals, Tokyo, 1982) p. 203.
22. K. H. J. BUSCHOW, *J. Phys. F Metal Phys.* **13** (1983) 563.
23. A. J. PEDRAZA, M. J. GOODBOLE, E. A. KENIK, D. F. PEDRAZA and D. H. LOWNDES, in "Proceedings of the Materials Research Society Symposium (Materials Research Society, Pittsburgh, PA, 1987) Vol. 74, p. 185.
24. D. F. PEDRAZA, *Metall. Trans.* **21A** (1990) 1809.
25. L. J. SWARTZENDRUBER, V. P. ITKIN and C. B. ALCOCK, *J. Phase Equilibria* **12** (1991) 288.
26. Y. GROS and J. PAULEVE, *J. de Physique* **31** (1970) 459.
27. L. NÉEL, J. PAULEVE, R. PAUTHENET, J. LAUGIERT and D. DAUTREPPE, *J. Appl. Phys.* **35** (1964) 873.
28. J. I. GOLDSTEIN and D. B. WILLIAMS, in "Proceedings of the International Conference on Solid/Solid Phase Transformations" (TMS-AIME, Warrendale, PA, 1982) p. 715.
29. G. HAUSCH and H. WARLIMONT, *Phys. Lett.* **36A** (1971) 415.
30. K. B. REUTER, D. B. WILLIAMS and J. I. GOLDSTEIN, *Metall. Trans.* **20A** (1989) 719.
31. Y.-Y. CHUANG, Y. A. CHANG, R. SCHMID and J.-C. LIN, *ibid.* **17A** (1986) 1361.
32. A. WIEDENMANN, W. WAGNER and H. WOLLENBERGER, *J. Less-Common. Metals* **145** (1988) 47.
33. M. R. GALLAS, L. AMARAL and J. A. H. DA JORNADA, *J. Appl. Phys.* **70** (1991) 131.
34. F. A. GARNER, J. M. McCARTHY, K. C. RUSSELL and J. J. HOYT, *J. Nucl. Mater.* **205** (1993) 411.
35. O. BOSTANJOGLO and W. GIESSE, *Phys. Status Solidi (a)* **32** (1975) 79.
36. E. P. BUTLER and J. F. ORCHARD, in "Phase Stability During Irradiation", edited by J. R. Holland, L. K. Mansur, and D. I. Potter (TMS-AIME, Warrendale, PA, 1981) 315.
37. M. F. SINGLETON and P. NASH, in "Phase Diagrams of Binary Nickel Alloys", edited by P. Nash (ASM International, Materials Park, OH, 1991) p. 207.
38. H. OKAMOTO, *J. Phase Equilibr.* **12** (1991) 703.
39. B. C. GIESSEN, in "Proceedings of the Fourth International Conference on Rapidly Quenched Metals", edited by M. Masumoto and K. Suzuki (Japan Institute of Metals, Tokyo, 1982) p. 213.
40. E. D. WANG, G. X. LIANG and S. S. FANG, *Powder Metall. Technol.* **12** (1994) 171.
41. Z. J. ZHANG and B. X. LIU, *J. Phys. Condens. Matter.* **7** (1995) L293.
42. B. X. LIU, *Phys. Status Solidi* **94a** (1986) 11.
43. J. A. ALONSO, L. J. GALLEGO, J. A. SOMOZA and B. X. LIU, "Thin Films and Beam–Solid Interactions", edited by L. Huang (Elsevier, Amsterdam, 1991) 297.
44. H. MORI, H. FUJITA, M. TENDO and M. FUJITA, *Scripta Metall.* **18** (1984) 783.
45. S. BANERJEE, K. URBAN and M. WILKENS, *Acta Metall.* **32** (1984) 299.
46. M. YAMAMOTO, S. NENNO and Y. HOMNA, in "In Situ Experiments with HEVM", Proceedings of the International Symposium on the Behaviour of Lattice Imperfections in Materials, edited by H. Fujita (Osaka University, 1985) p. 287.

*Received 6 February*
*and accepted 8 May 1996*